Stability Analysis of Motor Drive Interactions in Aircraft Electrical systems

C.E. Jones[1], M. Barnes[2], A.J. Forsyth[3]

1. Department of Electronic and Electrical Engineering
University of Strathclyde
Royal College Building,
204 George Street
Glasgow G1 1XW
Tel: +44(0) 141 548 2715
Fax: +44(0) 141 552 2487
E-mail:catherine.jones@eee.strath.ac.uk
2. Sackville Street Building-A13b
School of Electrical and Electronic Engineering
The University of Manchester
Manchester
M13 9PL
Tel: +44(0)161 306 4798
E-mail: m.barnes@manchester.ac.uk
3. Sackville Street Building-A5
School of Electrical and Electronic Engineering
The University of Manchester
Manchester
M13 9PL
Tel: +44(0)161 306 4675
E-mail: andrew.forsyth@manchester.ac.uk

Acknowledgements

The authors would like to acknowledge the financial support from the European Union Framework 6 More Open Electric Technologies (MOET) project.

Keywords

<< Permanent magnet motor, Multi-machine system, Control of drive, Airplane >>

Abstract

More Electric Aircraft are currently being developed so that in the future all non-propulsive power on an aircraft can be provided by the electrical system. In this electrical system, it is expected that several motor loads will run in parallel from a single DC bus. The paper will investigate the interactions between five motor loads connected to a common DC bus, paying particular attention to the effects of the line impedance on the stability of the system, and how this interacts with any capacitance in the input filters to the motor drive loads. Based on the results of the tests carried out, guidelines to ensure the stability of a multiple load system are presented.

To achieve this, a generic model for a motor load is proposed. Five of these motor loads are then connected to a DC bus and the stability of this system has been tested. The motor parameters have been scaled to represent models of different sizes, and they have different input filters. The impedance of the line has been included.

Nomenclature

L:	inductance	[H]
R:	resistance	[Ω]
Ψ:	flux	[V/m]

ω_r:	electrical speed	[rad/s]
ω:	mechanical speed	[rad/s]
ω_n:	bandwidth of controller	[rad/s]
P_T:	pole pairs	[-]
J:	inertia	[kg.m^2]
H:	inertia constant	[MW.s/MVA]
ζ:	damping constant	[-]
T_e:	electrical torque	[N.m]
T_l:	mechanical torque	[N.m]

1. Introduction

There is strong motivation to develop More Electric Aircraft (MEA), on which all non-propulsive power can be supplied by the electrical system [1], replacing the hydraulic, pneumatic and mechanical power systems on a conventional aircraft. While MEA will be more efficient, reliable and easier to maintain than a conventional aircraft [2-4], this is achieved by greatly increasing the complexity of their electrical power system. Conventional electrical systems on aircraft were single frequency [2,5] with a load of around 100kW [2]. An MEA will require up to 1.6MW for a 300 passenger (pax) aircraft [2], with a complex electrical network consisting of a mixture of AC and DC, with varying voltage and frequency levels. It is highly likely that part of such a complex network will include several motor loads, supplied by a single DC bus, as shown by Fig. 1. Some of these loads, such as the environmental control system, will have a power rating which is a significant proportion of the generator rating. As a result there is a high potential for interactions between the individual motors and design rules must be formulated to ensure correct system operation under all conditions. The length of the DC distribution circuit could be up to 60m in length [6], therefore the line impedance of the DC bus must be considered, and may have a significant impact on the stability of the system.

This paper will describe how the model of the multiple load system was developed, validated, and subsequently used to investigate the stability and robustness of such a system, paying particular attention to the effects of the line impedance on the stability of the system, and how this interacts with any capacitance in the input filters to the motor drive loads. The multiple load system which has been considered is shown in Fig.1.

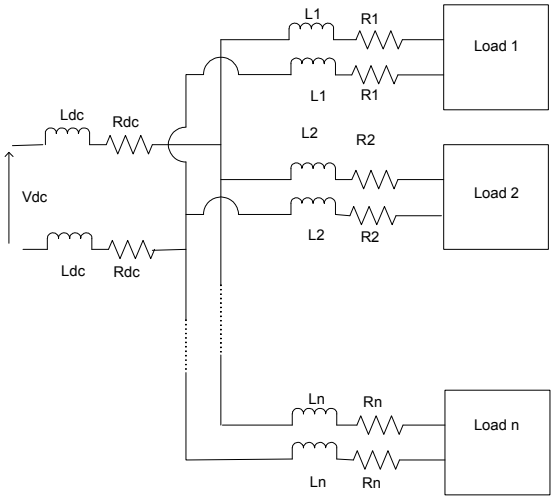

Fig. 1: Multiple motor loads on a DC bus.

2. General Model of Motor load

2.1 Overview of the Motor Load Model.

A generic model of a permanent magnet synchronous motor (PMSM), drive and associated control has been developed. Fig. 2 shows a block diagram of this model.

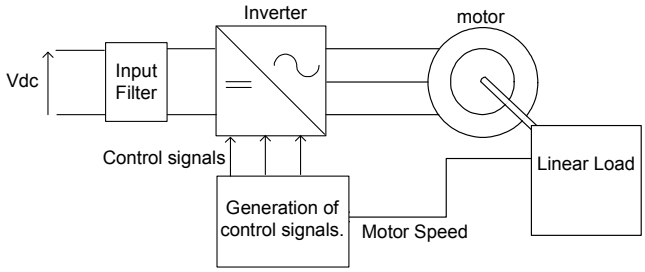

Fig.2: Block diagram of PMSM load, comprising motor, motor drive, control and linear load.

2.2 The Permanent Magnet Synchronous Motor Model

The PMSM has been modelled in d-q form. Assumptions which have been made are [6,7]:

- Saturation is neglected
- The induced EMF is sinusoidal
- Eddy currents and hysteresis loses are negligible
- There are no field current dynamics
- There is no cage on the rotor
- The rotor is made from permanent magnet material or is energised with constant field current i.e. the rotor contribution to magnetic flux linkage is constant
- The magnetic system is linear.
- The system is balanced and hence may be modelled by abc to dq transforms (rather than abc to dq0 transforms).
- The stator windings are sinusoidaly distributed.
- The motor airgap is uniform
- The motor has saliency.
- The motor is a fault tolerant machine.

The machine has been modelled using the version of the d-q transformation described and derived in [6]. It should be mentioned that the synchronous machine described in [6] is a wound rotor machine. The magnitude invariant version of the three phase to d-q transform has been used. Equations 1 and 2 were derived to describe the d-q equivalent circuit of the PMSM.

$$v_q = \frac{d\Psi_q}{dt} + i_q R + \omega_r \Psi_d, \quad \frac{d\Psi_q}{dt} = L_q \frac{di_q}{dt}$$

$$\therefore v_q = L_q \frac{di_q}{dt} + i_q R + \omega_r (L_d i_d + \Psi_r) \tag{1}$$

$$v_d = \frac{d\Psi_d}{dt} + i_d R - \omega_r \Psi_q, \quad \frac{d\Psi_d}{dt} = L_d \frac{di_d}{dt}$$

$$\therefore v_d = L_d \frac{di_d}{dt} + i_d R - \omega_r \Psi_q \tag{2}$$

Equation 3 was derived to express the electric torque in the model from standard power-torque-speed relationship [8].

$$T_e = \frac{3}{2}\frac{\omega_r}{\omega}\left[(L_d - L_q) i_q i_d L + \Psi_r i_q\right]$$
$$= \frac{3}{2} P_T \left[(L_d - L_q) i_q i_d L + \Psi_r i_q\right] \tag{3}$$

2.3. The Motor Drive and Control

The control system developed follows a standard d-q cascaded controller methodology [9], with an inner and outer control loop. The outer, or speed, control loop regulates the shaft speed of the motor and generates a reference i_q for the inner control loop. The inner, or current, control loop generates the control signals for the generation of PWM signals to control the inverter, and hence the current to the motor. The d component of the current is controlled to be zero. The d and q loops have been decoupled using Equations 4 and 5.

$$v_{d-decoupling} = \omega_r \Psi_q \tag{4}$$

$$v_{q-decoupling} = -\omega_r (L_d i_d + \Psi_r) \tag{5}$$

Feed-forward DC link voltage control has been implemented within the inverter block, which is contained within the current loop control. In this feed-forward control, the per unit control voltage is compared to the triangular waveform with an amplitude of +/- 1, to generate the PWM waveforms to control the inverter. Variations in DC link voltage are thus rapidly compensated.

In order to tune the control loops the bandwidth and damping of the inner and outer loops are chosen, and from these chosen parameters, the values of the proportional and integral gains in the PI controllers are calculated. Fig. 4a and Fig.4b show the speed and current control loops.

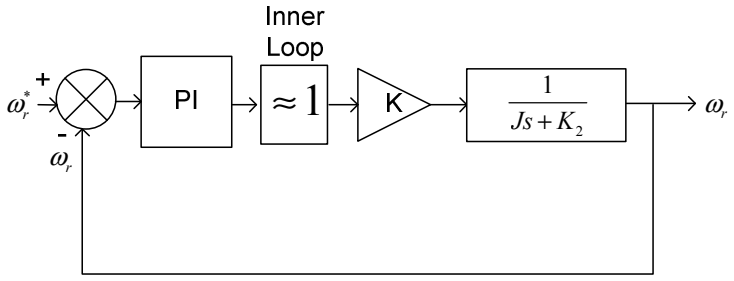

Fig. 4a: Speed control loop block diagram.

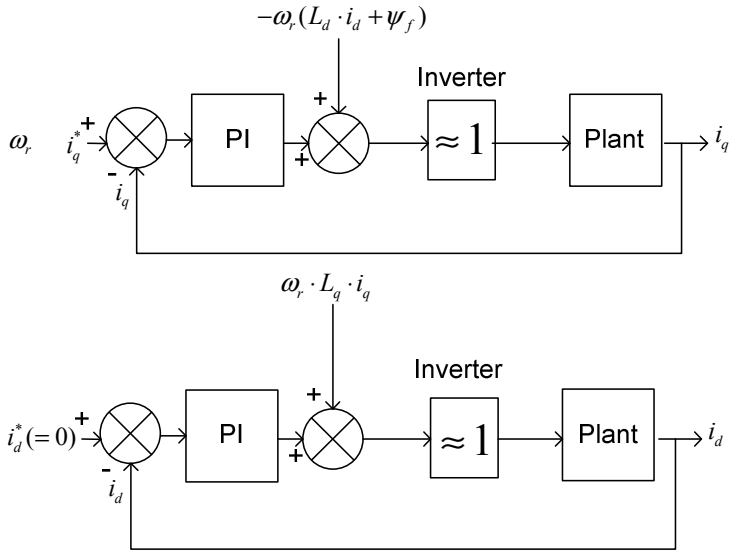

Fig. 4b: Current control loop block diagrams.

The bandwidth of the control loops is limited by the switching frequency of the inverter, the speed of the transducer in the physical system and the DC link voltage. Additionally the bandwidth of the inner loop should ideally be an order of magnitude, or more, larger than the outer loop. This results in a set of control loops which may, in principle, be tuned independently. The transfer function of the inner loop is given by Equation 6 and the transfer function of the outer loop is given by Equation 7. The input filter to the inverter was neglected when the inner loop was modelled. Equation 8 is a standard second order equation for a closed loop transfer function [10]. By inspection, if the effect of the right-hand term of Equations 6 and 7 is considered negligible and therefore only the left-hand term of each equation is considered, then Equations 6 and 7 can be seen to be of a similar form to Equation 8. Therefore the proportional and integral gains, ki and kp, for both the inner and outer loops can be calculated from Equations 6 and 7, for a chosen bandwidth, ω_n, and damping, ζ. Table I summarises the equations that are used to calculate the proportional and integral gains of the controllers.

$$H(s) = \frac{\frac{1}{L}\left(sK_p + K_i\right)}{s^2 + \left(\frac{R + K_p}{L}\right)s + \frac{K_i}{L}}$$

$$= \frac{\frac{1}{L}sK_p}{s^2 + \left(\frac{R + K_p}{L}\right)s + \frac{K_i}{L}} + \frac{\frac{1}{L}K_i}{s^2 + \left(\frac{R + K_p}{L}\right)s + \frac{K_i}{L}} \quad (6)$$

$$G(s) = \frac{\frac{K}{J}(sK_p + K_i)}{s^2 + s\left(\frac{K_2}{J} + \frac{KK_p}{J}\right) + \frac{KK_i}{J}}$$

$$= \frac{\frac{K}{J}sK_p}{s^2 + s\left(\frac{K_2}{J} + \frac{KK_p}{J}\right) + \frac{KK_i}{J}} + \frac{K_i\frac{K}{J}}{s^2 + s\left(\frac{K_2}{J} + \frac{KK_p}{J}\right) + \frac{KK_i}{J}} \quad (7)$$

$$Y(s) = \frac{\omega_n^2}{s^2 + 2\omega_n\zeta s + \omega_n^2} \quad (8)$$

Table I: Formulae for calculating proportional and integral gains in the control loops.

Control Loop	Ki	Kp
Speed	$\frac{\omega_n^2 J}{K}$	$\frac{J2\zeta\omega_n - K_2}{K}$
Current	$L\omega_n^2$	$2\omega_n\zeta L - R$

2.4 Validation of the Motor Load Model

In order to validate the control, the speed and current control loops were modelled using physics-based electrical model simulation and comparing the response to a simplified analytical representation. A step change was applied with three different levels of damping, for both control loops. Red traces are the response with a damping of 1, green traces are the response with a damping of 0.7 and blue are the response with damping of 0.2. By inspection of Figs. 5a and 5b, it can be see that for both control loops, there is good correlation between the results obtained from the electro-mechanical system model (left hand plots) and the mathematical equation based model (right hand plots). The switching inverter was replaced by a voltage source and the cross-coupling and decoupling equations were omitted in electro-mechanical model when testing the inner control loop. Including these affects the response, because the step in current is so small compared to the magnitude of the current flowing in the model.

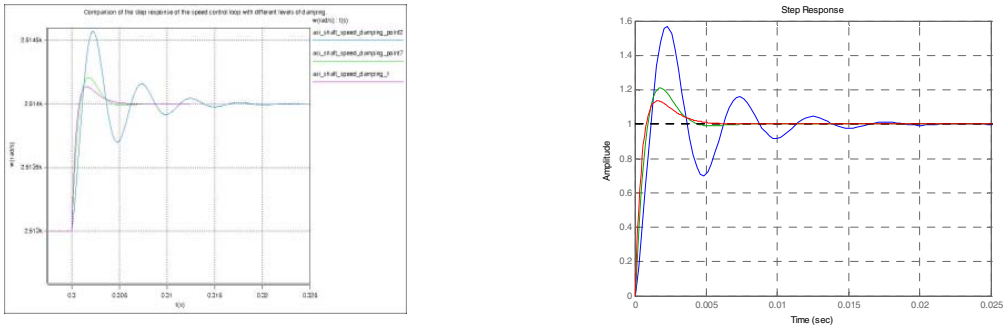

Fig. 5a: Validation of the speed control loop.

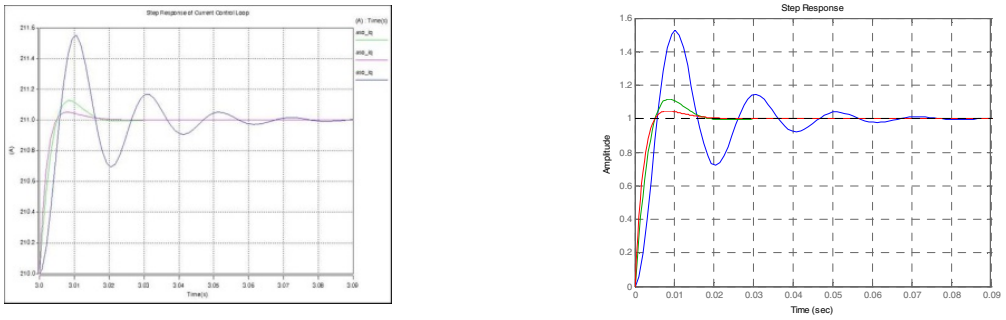

Fig. 5b: Validation of the current control loop.

3. DC bus with Multiple Loads

3.1 Overview of the Multiple Load Model

In order to study the stability of several of these motors connected to a DC bus, five motors were connected in parallel to a DC bus, simulating a possible section of the electrical architecture on an MEA. A model with 5 loads in parallel to the DC bus is large and complex to simulate. In order to simplify the multiple load model, the four smaller motors were combined to form an aggregate motor, to be run in parallel with the largest (150kW) motor, as shown in Fig. 6.

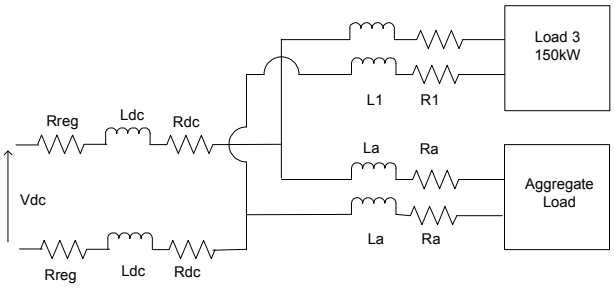

Fig. 6: Multiple load model with largest load and aggregate load.

3.2 Calculation of Model Parameters

The parameters of the five motors and the aggregate motor have been calculated by scaling the parameters of the initial motor, used to develop the motor model, on a per-unit basis using Equation 9. It was assumed that the back emf of the motors was constant at 190V. The motor inertia was scaled using Equation 10 [6]. The motor parameters were scaled using a base of 63kW and a base mechanical speed of 2513 rad/s. All motors are 2 pole pair machines. Table II gives the scaled motor parameters which were calculated and used in the simulations, including the parameters for the aggregate load.

$$Z_b = \frac{V^2}{P}, \qquad (9)$$

$$H = \frac{1}{2}\frac{J\omega_{mech}^2}{VA_b} \quad (10)$$

The impedance of the line has been estimated by considering the line to be a standard airframe wire, current ratings for different AWG gauges were found for a commercial aerospace wire [11]. The connecting wire from the DC bus to the motor loads was considered to be a go–and-return circuit. . The inductance for this was calculated using Equation 13 [12,13], where the self and mutual inductances were calculated using Equations 11 and 12 respectively [12,13]. The gauge of each wire was chosen based on the rated DC current supplied to each particular motor. Tables III and IV give details of the values calculated and used for the line impedance in the simulation models. The distance between the go and return wires was set to 1cm. Line resistance was modelled using values considered typical for an MEA. The distances between the wires supplying the individual motors were varied between three distances of 5m, 10m and 60m. These lengths would not be unreasonable to consider on a typical 300pax aircraft, which has a fuselage length of circa 63m and wing span of circa 60m [14].

$$L = 0.002l\left[\ln\frac{2l}{\rho} - \frac{3}{4}\right] [\mu H/m] \quad (11)$$

$$M = 0.002l\left[\ln\frac{2}{d} - 1 + \frac{d}{l}\right] [\mu H/m] \quad (12)$$

$$L_{go-return} = 2L - 2M \ [\mu H/m] \quad (13)$$

Where: l - length of wire [cm]
ρ - wire radius [cm]
d - distance between wires [cm]

Table II: Scaled motor load parameters

Motor Load	1	2	3	4	5	Aggregate
Motor Power [kW]	30	100	150	12	120	261.85
Electrical frequency [Hz]	1767	1800	1000	600	100	1291.74
Resistance [Ω]	0.0147	0.0044	0.0029	0.0369	0.0037	0.00169
Inductance [μH]	57.2	16.85	20.06	420.64	25.27	8.96
Flux Constant [v/rad/s]	0.01711	0.0168	0.0302	0.0503	0.0302	0.0234
Inertia [kg/m^2]	0.2m	0.627m	3m	0.677m	2.4m	3.2m

.

Table III: Line resistances and inductances for running 150kW and aggregate load in parallel.

Load Feeder		Resistance [mΩ]				Inductance [μH]	
		Line Length:				Line Length:	
	AWG	5m	10m	60m	5m	10m	60m
150kW Load	2/0	1.5	3	18	1	2	12
Aggregate Load	4/0*	0.5	1	6	0.38875	0.7775	4.665

*Two 4/0 wires were run in parallel due to high currents.

Table IV: Line resistance and inductances for running 5 motor loads in parallel on 10m long lines.

Load Feeder	AWG	Inductance [μH]	Resistance [mΩ]
1	10	4.5696	39
2	1	2.4826	5
3	2/0	2	3
4	10	4.5696	39
5	0	11.25	4

Additionally regulation resistance, Rreg, was included on the DC link bus connecting to the loads. This was calculated to be 0.35mΩ, based on a 0.1% variation in voltage at a full load of 410kW on the +/- 270V dc link.

Fig.7 shows the architecture of the input filter. The parameters of the filter components for the different motors are given in the appendices. Values considered typical for the input filters and the switching frequencies of the PWM were chosen. Table VI gives details of the filter parameters used.

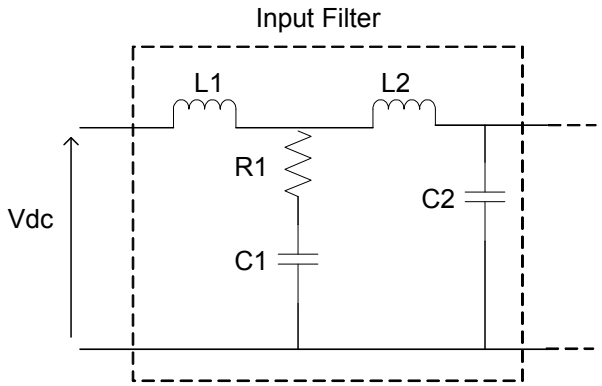

Fig. 7: Input filter architecture.

Table VI: Input Filter Parameters

Load	1	2	3	4	5	Aggregate
PWM Swtiching Frequency [kHz]	20	40	24	10	30	25
L1 [μH]	20	10	10	60	10	25
L2 [μH]	0	20	13	200	13	58.25
R [Ω]	0.3	0	0	0	0	0.075
C1 [μH]	1500	680	4700	0	4700	1720
C2 [μH]	80	420	630	280	630	352.5

4. Stability Studies

4.1 Stability Tests

To test the stability of the system, a load change of 5% was applied to the largest motor (150kW) after 0.6s. To apply the load change, the motor speed set point was adjusted to give a 5% increase in the load power drawn. The load change enabled the investigation of the effects of both the input filter to the motor drive and the amount of impedance in the line to the motor to the overall stability of the system.

It was found to be necessary to set the bandwidth of the controller to be low, 1000 rad/s for the inner loop and 100 rad/s for the outer loop in order to successfully execute the step change. If the bandwidth was set too high then the controller was found to saturate and unable to pull enough voltage from the DC link in response to the step change to the load. The DC link current and voltage to each load was measured at the terminals of the motor load module.

4.2 Results

The DC bus voltage and current to each motor load, alongside the speed of the 150kW motor were compared for each of the three models for each of the three feeder lengths, using the two generator aggregate model. Fig. 9a shows a comparison of the voltage, Figs. 9b and 9c show comparisons of the DC link current to the motor and Fig. 9d shows a comparison of the motor speed of the 150kW motor.

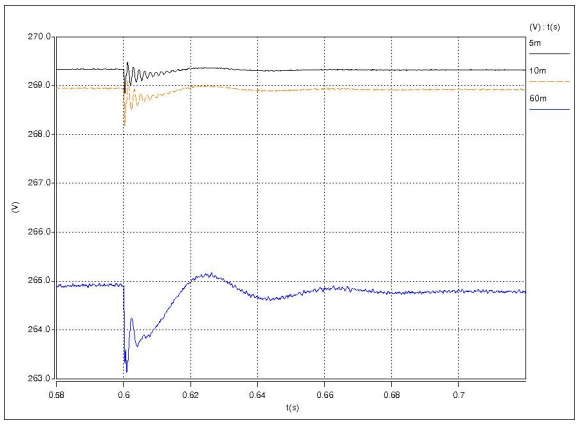

Fig.9a: DC link bus voltage

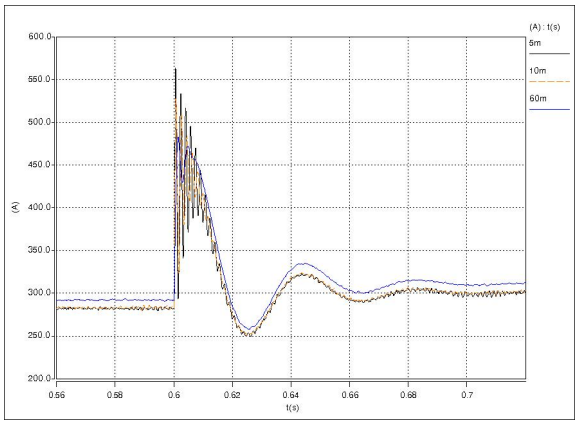

Fig. 9b: DC link current to 150kW load

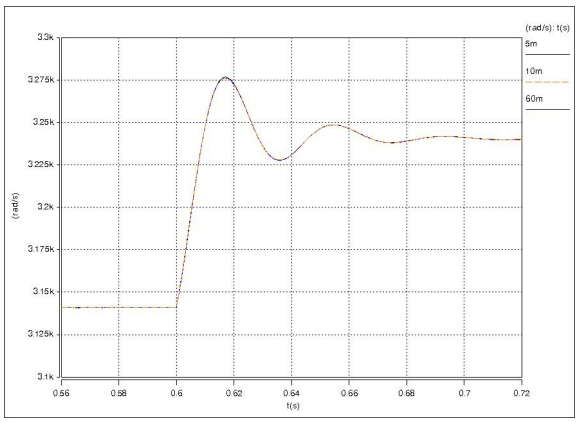

Fig. 9c: Speed of 150kW PMSM.

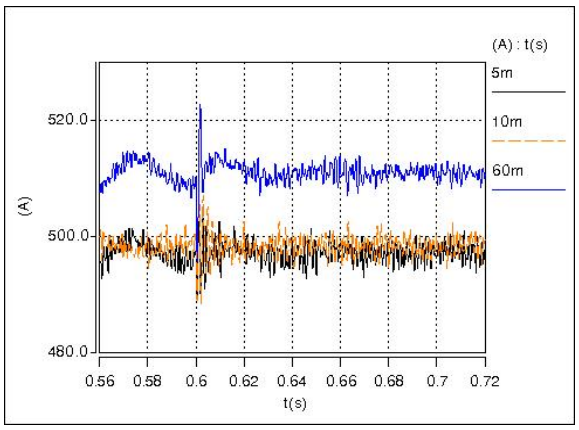

Fig. 9d: DC link current to aggregate load

By inspection of Fig.9a it can be seen that as the line length increases, although ringing increases with line length, it is does not become large enough to adversely affect the operation of the motors when a disturbance is applied to one motor.

However by inspection of Fig. 9b it can be seen that the response of the DC link current for the 5m and 10m line lengths, additionally contains the higher frequency oscillation due to the high capacitance of the input filter for the motor drive. The 60m response does not contain this high frequency oscillation due to the extra damping provided by the higher line resistance. Therefore results indicate that if the line resistance is below a certain threshold compared to the capacitance of the input filter, then unacceptable oscillations in the DC link current will result in the case of a disturbance occurring in the system.

Another effect of the input filter capacitance can be seen in Fig. 9c. It can be seen that although the damping for the speed control loop has been set to 1, the response is less damped. This is due to the response of the inner control loop to the sudden increase in the reference current, when the speed is subjected to a step change. The capacitance in the input filter is within the inner control loop. When the reference current to the inner control loop is subjected to a disturbance, the filter capacitance causes this oscillation, which is transferred to the speed because the current is used to calculate the load torque. Fig. 9d shows the DC link current to the aggregate load at the time of the step load increase to the 150kW load indicates that in general there is little disturbance to the operation of the aggregate load.

To validate the results from the aggregate load model, Fig. 11 shows a comparison between the 10m aggregate load model and 10m line five motor load model. Although the general dynamic behaviour of the DC link voltage is shown, there is more ripple in the 5 motor load model and the response is slightly slower due to the increased complexity of the 5 load model. The aggregate model is a representation of the average of the four smaller models and hence it would be extremely difficult to get better correlation than has been obtained. Moreover, it is the dynamics and response of the system to a disturbance on the 150kW load that is being primarily investigated, and

the dynamic response for the current, voltage and speed in both the aggregate and 5 load models are almost identical.

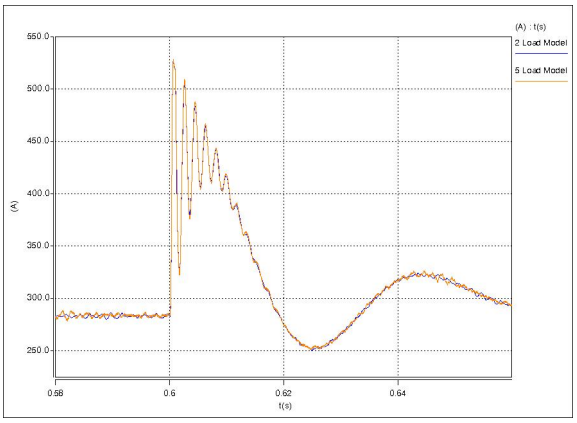

Fig.11a: Comparison of DC link current

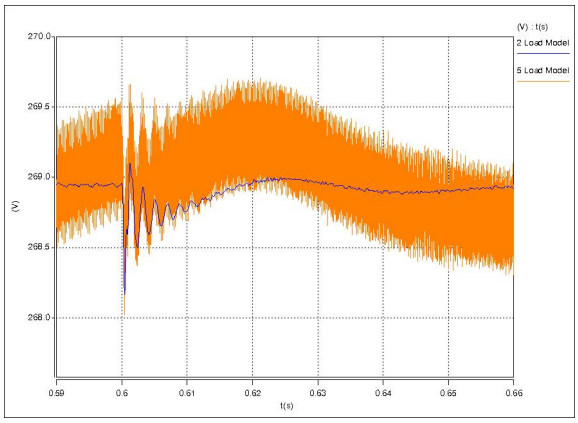

Fig.11b: Comparison of DC link voltage

5. Conclusions

A generic model of a motor load for an MEA has been developed and the control and model validated. Several motor loads have been scaled to different sizes and connected to a DC busbar and a disturbance applied. It is clear from results that the system is robust enough that a disturbance on one motor does not affect the DC bus voltage for the other motors.

The results presented in this paper have indicated that if there is significant capacitance present in the input filter for a motor load, then the line resistance is needed to damp the effects of this large capacitance. As line resistance increases with line length, then for certain input filter parameters, a system may not be sufficiently robust to disturbances if the length of the lines are too short. In addition the filter capacitance will affect the response of the inner control loop. Therefore whilst it was found to be necessary to set the bandwidth of the controller to be low to ensure that the controller did not saturate, in order to fully investigate the upper limit of the bandwidth that can be applied to the inner control loop, the input filter must be taken into account in the future.

References

[1] J.A. Weimer, The Role of Electrical Machines and Drives in a More Electric Aircraft, IEEE Electric Machines and Drives Conference, vol. 1, pages 11-15, 2003.
[2] C.R Avery et al, Electrical Generation and Distribution for the More Electric Aircraft, UPEC, 2007, Pages 1007-1012.
[3] A. Emadi and M. Ehsani, Aircraft Power Systems: Technology, State of the Art and Future Trends, IEEE AES Systems Magazine, issue 1, Pages 28-32, 2000.
[4] J.A. Rosero et al, Moving Towards a More Electric Aircraft, IEEE A&E Systems Magazine, March 2007, Pages 3-9.
[5] I. Moir, A. Seabridge, Aircraft Systems, 3rd ed., Wiley, 2008.
[6] P. Kundur, Power System Stability and Control, McGraw-Hill, 1993.
[7] A. E. Fitzgerald et al, Electric Machinery, McGraw Hill, USA, 1992.
[8] P. Krause et al, Analysis of Electric Machinery and Drive Systems, IEEE Press, USA, 2002.
[9] P.Pillay, R. Krishnan, Modelling of Permanent Magnet Motor Drives, IEEE Transactions on Industrial Applications, Vol. 135, No. 4, November 1988.
[10] D. K. Anand, R. B. Zmood, Introduction to Control Systems, Butterworth-Heinemann, UK, 1995
[11] Flame resistant airframe wires according to NSA935-131 DG, AIR 1715 series, www.draka.fr, website visited March 2009.
[12] F.W. Grover, Inductance Calculations, Dover Publications, USA, 1962.
[13] E.B. Rosa, The Self and Mutual Inductances of Linear Conductances, Bulletin of the Bureau of Standards, Vol. 4, No. 2, Page 301, 1908.
[14]Dimensions of an A330 aircraft, www.airbus.com/en/aircraftfamilies/productcompare, website visited June 2009.